

Article

Paleoproterozoic Mineralization of the Lijiapuzi Gold Deposit in the Liaodong Peninsula, NE China: Constraints from ^{40}Ar - ^{39}Ar Age, S-Pb Isotopes, and In Situ Analyses

Yan Zhao ^{1,2,*}, Peng Zhang ^{1,2}, Hongzhi Yang ^{1,2}, Linlin Kou ^{1,2}, Zhongwei Bi ^{1,2}, Zhongzhu Yang ^{1,2} and Jiang Chen ¹

¹ Shenyang Center, China Geological Survey, Shenyang 110034, China; geozhangpeng2010@163.com (P.Z.); yangxx272000@163.com (H.Y.); koulinlin@126.com (L.K.); bizhongwei@mail.cgs.gov.cn (Z.B.); yangzhongzhu@mail.cgs.gov.cn (Z.Y.); hardrock30@163.com (J.C.)

² Key Laboratory of Deep Mineral Resources Exploration and Evaluation, Department of Natural Resource of Liaoning Province, Shenyang 110032, China

* Correspondence: zhaoyan@mail.cgs.gov.cn

Abstract: A Paleoproterozoic $^{40}\text{Ar}/^{39}\text{Ar}$ age, interpreted as the gold metallogenic epoch of the Lijiapuzi deposit in NE China, is reported in this paper. The ore body of this deposit is hosted in the marbles and schists of the Paleoproterozoic Dashiqiao Formation and exhibits parallel development to the foliation of the country rocks. Coexisting auriferous pyrite and tremolite can be observed both in the field and under a microscope, revealing the presence of hydrothermal activity in the deposit. The $\delta^{34}\text{S}$ composition of the auriferous pyrite varies from +8‰ to +12.3‰, indicating a sedimentary origin. The auriferous pyrite and host marble have similar Pb isotopic ratios, indicating the contribution of Paleoproterozoic sediments to gold mineralization. Furthermore, in situ S and trace element analyses of the auriferous pyrite reveal that the main gold mineralization stage was Py2, which coexists with radial tremolite. $^{40}\text{Ar}/^{39}\text{Ar}$ dating of these tremolite samples yields a plateau age of ~1851.23 Ma, with similar isochronal and inverse isochronal ages. The Paleoproterozoic gold metallogenesis, together with the contemporary Pb-Zn, boron, graphite, and magnetite mineralization, constitute an important mineralogenetic series during the evolution of the Jiao-Liao-Ji orogeny in the Liaodong Peninsula.

Keywords: $^{40}\text{Ar}/^{39}\text{Ar}$ dating; in situ analysis; S-Pb isotopes; gold mineralization; Jiao-Liao-Ji orogeny; the Lijiapuzi deposit



Citation: Zhao, Y.; Zhang, P.; Yang, H.; Kou, L.; Bi, Z.; Yang, Z.; Chen, J. Paleoproterozoic Mineralization of the Lijiapuzi Gold Deposit in the Liaodong Peninsula, NE China: Constraints from ^{40}Ar - ^{39}Ar Age, S-Pb Isotopes, and In Situ Analyses. *Minerals* **2022**, *12*, 971. <https://doi.org/10.3390/min12080971>

Academic Editor: Dominique Gasquet

Received: 22 June 2022

Accepted: 26 July 2022

Published: 29 July 2022

Publisher's Note: MDPI stays neutral with regard to jurisdictional claims in published maps and institutional affiliations.



Copyright: © 2022 by the authors. Licensee MDPI, Basel, Switzerland. This article is an open access article distributed under the terms and conditions of the Creative Commons Attribution (CC BY) license (<https://creativecommons.org/licenses/by/4.0/>).

1. Introduction

The Liaodong Peninsula in the northeastern part of the North China Craton (NCC) has a long history of geological evolution. The peninsula consists of an Archean crystallized basement, Paleoproterozoic meta-sedimentary rocks, and an orogenic belt (Figure 1a) [1–4]. Multiple mineral resources, including gold, lead, zinc, boron, magnesite, and graphite, were formed during the early geological process, forming the important Liaodong-Ji'nan metallogenic belt [5–10]. Due to the significant gold reserves in the main gold orefields, such as the Qingchengzi, Maoling, and Wulong orefields, the Liaodong Peninsula possesses one of the most important gold producing areas in China. The Qingchengzi orefield, with a total gold reserve of over 200 t [11,12], still has gold exploration potential. The Lijiapuzi gold deposit to the north and the deep gold ore bodies in the Baiyun and Linjiasandaogou deposits are newly discovered.

Many studies have focused on the metallogenesis of the Qingchengzi gold deposits; however, their conclusions remain controversial. The model of metamorphic–sedimentary processes imposed by late hydrothermal activities is preferred [14–18] since the gold ore bodies often exhibit the same attributes as the Liaohe Group country rocks, and the

geochemistry of the country rocks and ore-bearing minerals are similar. Others have reported the presence of Mesozoic magmatism and some mineralized dykes within this district [19–22]. They believe that the gold deposits are magmatic–hydrothermal-related-type or decratonic-type deposits. Whether there is Paleoproterozoic gold mineralization remains one of the critical issues due to the lack of robust geochronological evidence.

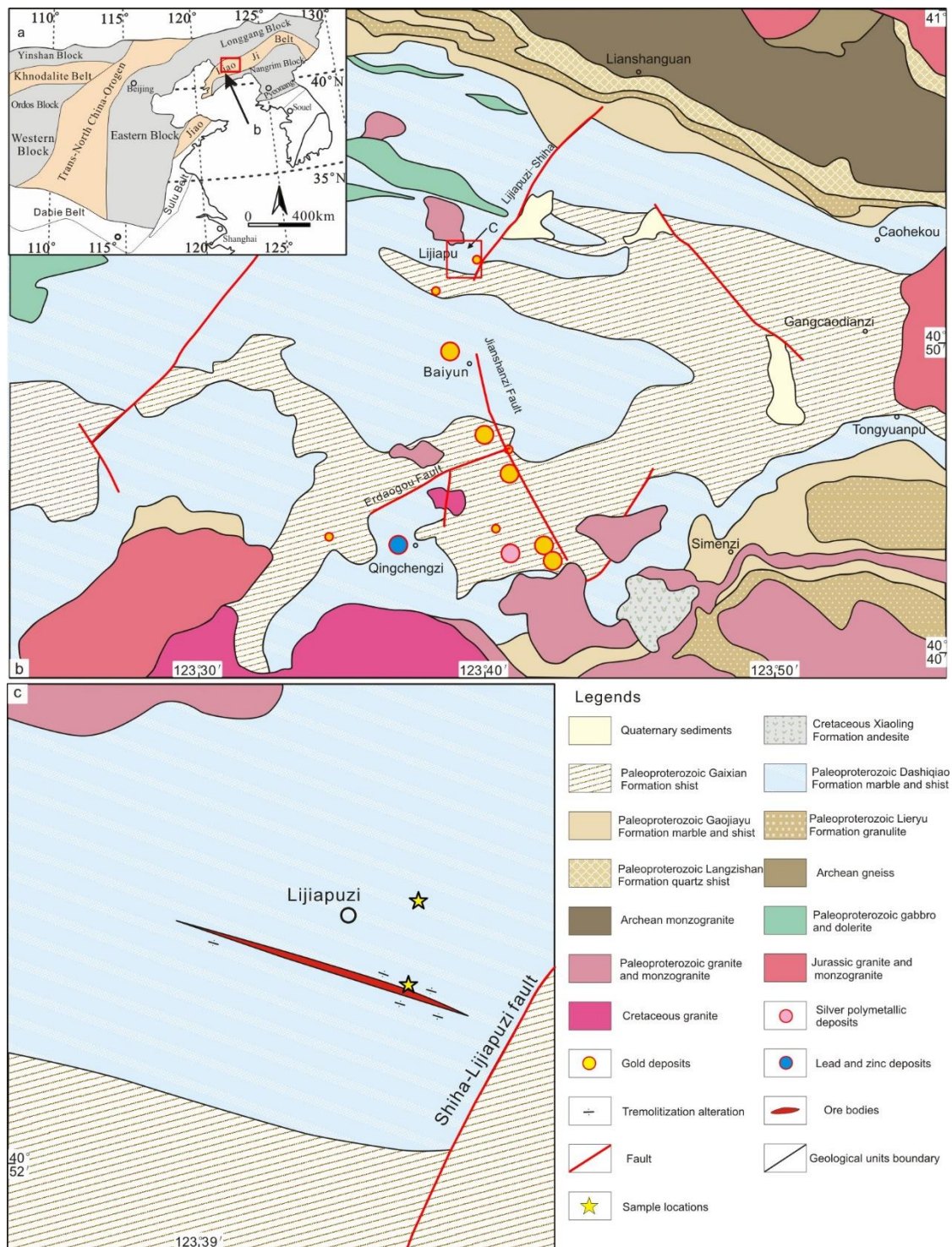


Figure 1. (a) Simplified tectonic map of partial North China Craton showing locations of the Liaodong Peninsula and the Jiao-Liao-Ji belt (modified after [2]). (b) Geological map of the Qingchengzi area showing major mineral deposits (modified after [13]). (c) Geological map of the Lijiapuzi gold deposit showing sample locations.

The newly discovered Lijiapuzi gold deposit was chosen as the object of this study. After detailed field and laboratory observations, important tremolitization accompanied by auriferous pyrite was identified, with euhedral radial tremolite. We conducted ^{40}Ar - ^{39}Ar dating of tremolite samples to precisely constrain the metallogenic epoch of the formation of the deposit. The S and Pb isotopes of auriferous sulfides and in situ laser ablation inductively coupled mass spectrometry (LA-ICP-MS) analyses of the S and trace element contents of the auriferous minerals were also conducted. Paleoproterozoic metallogenic evidence in the Lijiapuzi deposit and the related gold mineralization and ore material sources were obtained. The results of this study also expand the Paleoproterozoic mineralogenetic series in the Liaodong Peninsula.

2. Geologic Setting of the Qingchengzi Orefield

Located in the northeastern margin of the NCC (Figure 1a), the Liaodong Peninsula consists of the Archean Longgang Block, the Archean Nangrim Block, the Paleoproterozoic Jiao-Liao-Ji Belt (JLJB), and Mesozoic volcanic and granitic intrusions [1–4,23]. The JLJB orogeny involved the deposition of voluminous Paleoproterozoic sediments, including the Liaohe Group in the Liaoning Province, the Ji'an and Laoling groups in the Ji'lin Province, and the Jingshan and Fenzishan groups in the Shandong Province [24,25], as well as igneous and metamorphic rocks [26–29]. The marble and biotite schist of the Dashiqiao Formation and the schist of the Gaixian Formation are both components of the Liaohe Group, and they comprise the country rock in the Qingchengzi polymetallic orefield and nearby gold deposits. The NCC experienced strong magmatism again in the Mesozoic, which is referred to as the decratonic process [30].

The JLJB is NW–SE-trending and consists of intensely deformed geological units. There is a giant E–W-trending anticline in the Baiyun–Qingchengzi area in the central part of the JLJB. Other subordinate synclines and anticlines, including the Xinling and Zhenzigou anticlines, have also been identified within the Qingchengzi orefield. The fault structural framework is dominated by the NW-trending Jianshanzi Fault and the NE trending Erdaogou and Lijiapuzi–Shihazhai faults, as well as their related secondary faults. Almost all of the lead–zinc deposits are located to the south of the Erdaogou Fault, and a series of gold deposits are distributed along or to the west of the Jianshanzi Fault (Figure 1b).

The Paleoproterozoic magmatism in the Qingchengzi area resulted in widespread granitoid intrusions and sporadically distributed gabbros and dolerites. The Simenzi and Fangjiaweizi monzogranite plutons in the southeast intruded before ~2.16 Ga and ~1.89 Ga [31–33]. The Lanjiagou and Lanhualing Paleoproterozoic stocks are located in the central part of the Qingchengzi orefield (Figure 1b). These granitoids are believed to have intruded in an arc setting in the Paleoproterozoic [26]. The sporadic gabbro and/or dolerite dykes have been interpreted to be related to a Paleoproterozoic back-arc basin geological setting at ~2.11 Ga [34–36]. The Triassic Shuangdinggou and Xinling granite intrusions, which have U–Pb ages of ~225 Ma [6,37], correspond with the sporadic lamprophyre dykes in this area. Jurassic diorites and monzogranites with strong deformation have also been identified [18,23]. The Mesozoic magmatism has often been interpreted as the result of the subduction of the Yangtze Craton from the south [18,21].

A series of gold, Pb–Zn, B, and magnetite metallogenies are distributed within the JLJB in the Liaodong Peninsula [7,8,15,37–39]. Among the three famous Qingchengzi, Maoling, and Wulong gold orefields, only the Qingchengzi orefield hosts giant Au–Ag–Pb–Zn polymetallic deposits. Neither the Paleoproterozoic granitoids nor the Mesozoic intrusions exhibit gold mineralization in this area [40]. The marbles and schists of the Dashiqiao Formation and the schist of the Gaixian Formation comprise the country rocks of the gold ore bodies. The ore bodies often exhibit lens, stratiform, or irregular shapes, which are controlled by the host rocks and/or faults. Silicification, sericitization, tremolitization, and pyritization are the most common alterations within the gold deposits.

3. Sampling and Analytical Methods

The Lijiapuzi gold deposit, which consists of one gold orebody, is a small-scale deposit in the northern part of the Qingchengzi orefield. The gold ore body has an NW trend, which is parallel to the foliation of the marbles of the Dashiqiao Formation (Figure 1c). Although the ore body is distributed near the NE Shiha–Lijiapuzi Fault, the gold mineralization and the ore-bearing pyrite in this ore body seem to be related to the marble country rock and the tremolite alteration therein (Figure 2). The main ore minerals include pyrite, chalcopyrite, sphalerite, and galena. Early-stage pyrite (Py1), which has a euhedral shape, is often cracked when observed under a microscope. Late-stage pyrite (Py2), which has a relatively high gold content, is the main ore phase (Figure 3). Minor chalcopyrite and sphalerite are found in association with Py2 in the main mineralization stage. Tremolitization is a common type of alteration in this deposit, along with weak silicification, sericitization, and chloritization. Tremolite often cuts through the Py1 in the cracks (Figure 2f). Paragenesis of the Py2 and radial tremolite were observed under a microscope (Figure 2c).

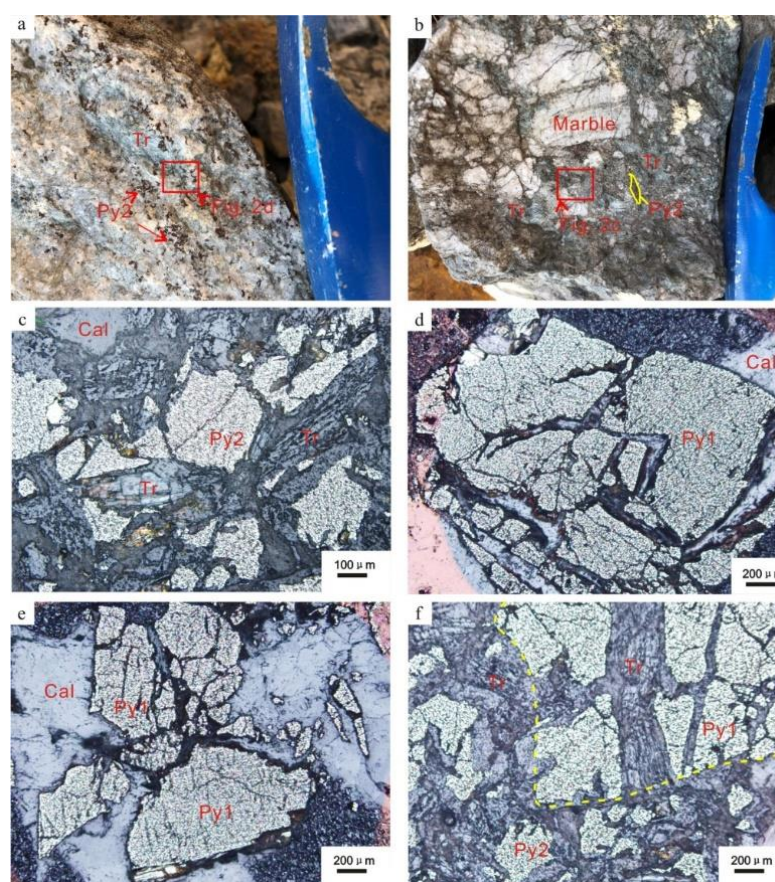


Figure 2. Representative outcrops and photomicrograph of ores from the Lijiapuzi gold deposit. (a,b) Field photos of Au-bearing pyrites and radial tremolite in country rock marbles. (c) Photomicrograph of ore-bearing pyrite and tremolite under a transmission ray. (d–f) Reflected light photomicrograph of different stages of ore-bearing pyrite. Cal—calcite; Py1—early-stage pyrite; Py2—late-stage pyrite; Tr—tremolite.

A tremolite sample (YP-9) that coexisted with the auriferous pyrite was collected for $^{40}\text{Ar}/^{39}\text{Ar}$ dating. Detailed S and Pb isotopic analyses were conducted on Au-bearing pyrite (Py2 type) samples (YP-1–YP-8) to study the ore-forming materials. In contrast, for determining a country rock's contribution to the mineralization process, marble samples (QC-1–QC-3) were chosen for Pb isotope analysis. In situ analysis of the S and trace element contents of seven samples was also conducted to analyze the precise textures and contents of the ore-bearing pyrite.

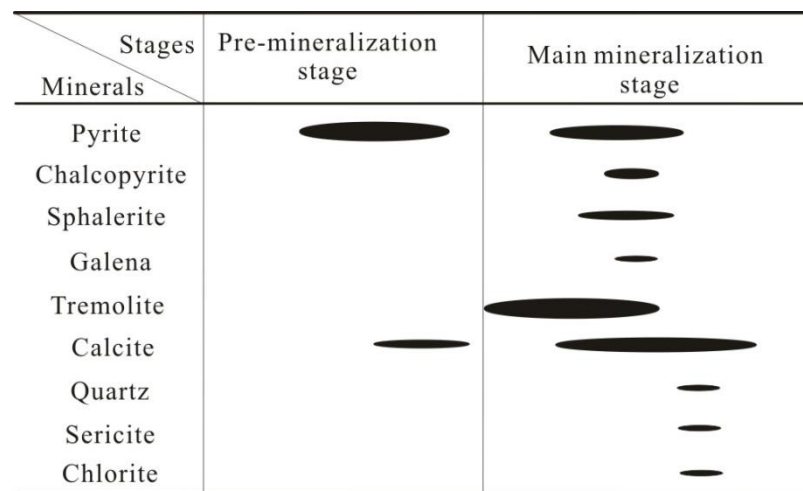


Figure 3. Paragenetic chart showing ore and gangue minerals in the Lijiapuzi gold deposit.

3.1. Tremolite $^{40}\text{Ar}/^{39}\text{Ar}$ Dating

The $^{40}\text{Ar}/^{39}\text{Ar}$ dating of the tremolite was performed at the Isotope Geology Laboratory, Institute of Geology Chinese Academy of Geological Sciences. For the tremolite analyses, we followed the procedure of Liu et al. [41]. The samples were loaded in aluminum packets and degassed at low temperatures (250–300 °C) for 20–30 min before being incrementally heated in a double-vacuum graphite furnace. The gases released during each heating step were purified using Ti and Al-Zr getters. Once cleaned, the gas was introduced into a GV Instruments HELIX-MC noble gas mass spectrometer and allowed to stabilize for 4–5 min before the static analysis was conducted. The ^{40}Ar , ^{39}Ar , ^{38}Ar , ^{37}Ar , and ^{36}Ar isotope abundances at time zero were obtained through linear extrapolation of the peak intensities. The data were corrected for system blanks, mass discrimination, Ca interference, K-derived argon isotopes, and the decay of ^{37}Ar since the time of irradiation. The decay constant used throughout the calculations was $\lambda = (5.543 \pm 0.010) \times 10^{-10} \text{ a}^{-1}$. All of the errors are reported as 2σ .

3.2. Pb isotope Analyses of Pyrite and Country Rock

Pyrite and country rock marble samples were collected from the Lijiapuzi deposit and nearby for Pb isotope analysis. The pyrite grains were sorted to a purity of 99% before applying the analysis procedures described by Zhang et al. [21]. The lead isotope compositions were analyzed via thermal-ionization mass spectrometry (TIMS; MAT-261), and standard sample NBS 981 was used for the calibration. The analyses were carried out at the Beijing Research Institute of Uranium Geology. The analytical precision of the Pb isotope ratios is better than $\pm 0.09\%$.

3.3. In Situ LA-ICP-MS S and Trace Element Analyses

In situ LA-ICP-MS trace element analysis of pyrite was conducted at the Wuhan Sample Solution Analytical Technology Co., Ltd., Wuhan, China. The laser sampling was performed using a GeolasPro laser ablation system (Coherent, Santa Clara, CA, USA), consisting of a COMPexPro 102 ArF excimer laser (wavelength of 193 nm and maximum energy of 200 mJ) and a MicroLas optical system. The spot size and frequency of the laser were set to 44 μm and 5 Hz, respectively. Detailed analysis procedures for determining the trace element compositions of sulfides were calibrated against various reference materials (NIST 610 and NIST 612) without using an internal standard [42]. Sulfide reference material MASS-1 (United States Geological Survey) was used as the unknown sample to verify the accuracy of the calibration method. Each analysis incorporated a background acquisition of approximately 20–30 s followed by 50 s of data acquisition from the sample.

4. Results

4.1. Tremolite ^{40}Ar - ^{39}Ar Dating

The ^{40}Ar - ^{39}Ar step-heating dating data for tremolite are presented in Table 1. Thirteen heating steps were carried out on the sample. Eight heating steps, with temperatures ranging from 1140 °C to 1400 °C, yielded a perfect plateau age of 1851.2 ± 12.8 Ma (Figure 4a). The data for the step heating from 1140 °C to 1400 °C yielded an isochronal age of 1857.88 ± 12.3 Ma, with a mean standard weighted deviation (MSWD) of 3.18 (Figure 4b), and an identical inverse isochronal age of 1858.44 ± 12.3 Ma, with an MSWD of 3.15 (Figure 4c). The plateau age of 1851.2 Ma is thus interpreted as the crystallization age of tremolite.

Table 1. ^{40}Ar - ^{39}Ar data of tremolite from the Lijiapuzi gold deposit.

T	$^{36}\text{Ar}[\text{V}]$	$^{37}\text{Ar}[\text{V}]$	$^{38}\text{Ar}[\text{V}]$	$^{39}\text{Ar}[\text{V}]$	$^{40}\text{Ar}[\text{V}]$	$^{40}\text{Ar}\text{R}\%$	$^{39}\text{Ar}(\text{K})\%$	Age/Ma	2σ
900 °C	47.310	0.000	9.185	7.748	17,939.35	22.07	0.53	1697.42	52.4
980 °C	19.591	0.000	4.136	15.393	13,359.54	56.67	1.05	1655.62	12.8
1040 °C	8.685	0.000	1.981	17.744	10,505.46	75.57	1.21	1555.05	7.7
1100 °C	3.625	19.219	1.701	25.299	15,020.56	92.88	1.73	1783.26	5.8
1140 °C	4.160	1001.696	4.544	95.651	56,828.54	97.96	6.47	1854.19	4.3
1170 °C	59.297	2617.420	19.292	216.178	141,105.48	87.71	14.61	1836.72	4.4
1200 °C	10.667	7530.800	24.868	573.805	337,662.80	99.22	38.74	1860.44	4.2
1230 °C	3.437	2467.695	8.135	192.399	112,562.07	99.25	12.99	1853.74	3.8
1250 °C	2.588	379.050	1.999	36.459	21,948.31	96.64	2.47	1853.62	5.0
1300 °C	10.647	855.654	5.222	75.926	47,304.14	93.48	5.13	1855.70	4.2
1350 °C	14.091	1662.685	8.132	135.668	82,704.71	95.11	9.17	1851.42	4.0
1400 °C	24.373	896.403	7.586	83.600	55,222.62	87.07	5.65	1840.72	4.9
1450 °C	35.321	0.000	6.190	3.828	11,291.97	7.57	0.26	938.41	119.1

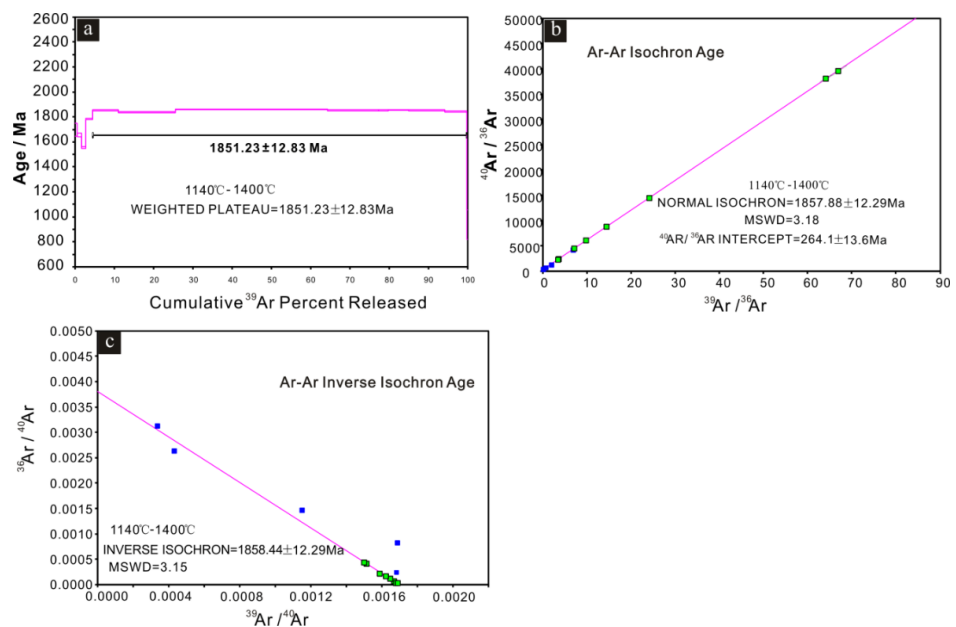


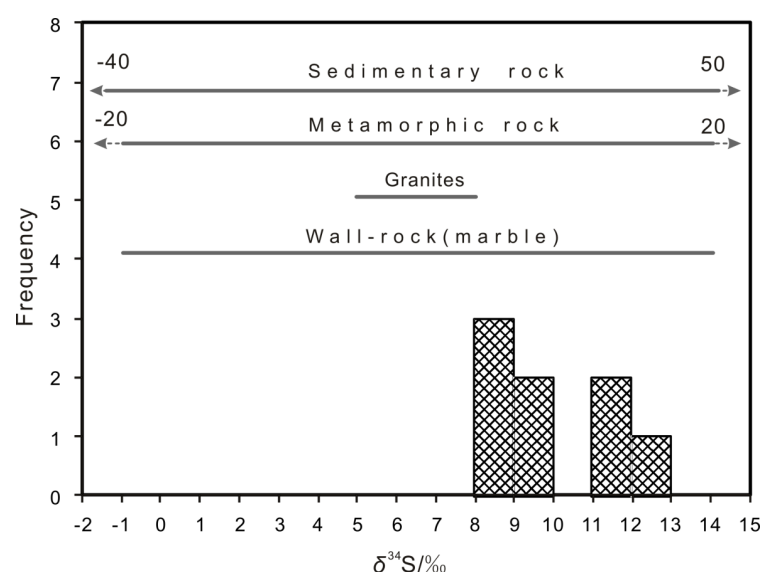
Figure 4. (a) ^{40}Ar - ^{39}Ar -weighted mean plateau age, (b) ^{40}Ar - ^{39}Ar isochronal line age, and (c) ^{40}Ar - ^{39}Ar inverse isochronal line age of tremolite samples.

4.2. S Isotope Composition of Auriferous Pyrite

The S isotope compositions of the auriferous pyrite samples are presented in Table 2. The $\delta^{34}\text{S}$ values are +8.0‰ to +12.3‰, which are higher than those of the granites (Figure 5). It is believed that the sulfur source of the metallogenic deposit was probably the nearby meta-sedimentary rocks of the Liaohe Group [15,19].

Table 2. Sulfur isotopic data of ore-bearing pyrite from the Lijiapuzi gold deposit.

Sample No.	Mineral	$\delta^{34}\text{S}/\text{‰}$
YP-1	Pyrite	9.8
YP-2	Pyrite	8.8
YP-3	Pyrite	12.3
YP-4	Pyrite	9.7
YP-5	Pyrite	11.3
YP-6	Pyrite	8.6
YP-7	Pyrite	8
YP-8	Pyrite	11

**Figure 5.** Sulfur isotope composition from the ore-bearing pyrite of the Lijiapuzi deposit sedimentary rocks, metamorphic rocks, granites, and wall–rock (marble) data from [43].

4.3. Pb Isotope Results

The Pb isotopic ratios of the Au-bearing pyrite and country rock marble are presented in Table 3. The pyrite exhibits $^{206}\text{Pb}/^{204}\text{Pb}$ ratios of 18.155 to 18.886, $^{207}\text{Pb}/^{204}\text{Pb}$ ratios of 15.594 to 15.687, and $^{208}\text{Pb}/^{204}\text{Pb}$ ratios of 38.26 to 39.695 (Figure 6). Meanwhile, the widespread marble in the Qingchengzi orefield area exhibits $^{206}\text{Pb}/^{204}\text{Pb}$ ratios of 21.822 to 23.035, $^{207}\text{Pb}/^{204}\text{Pb}$ ratios of 16.092 to 16.146, and $^{208}\text{Pb}/^{204}\text{Pb}$ ratios of 37.472 to 37.668 (Figure 6). The lead isotope ratios of the ore-bearing pyrite data were also plotted into the Liaohé Group country rock lead isotopic field, as previous studies have suggested [6,8,17,37].

Table 3. Lead isotope ratios of ore-bearing pyrites and marbles from the Lijiapuzi gold deposit.

No.	Target	$^{206}\text{Pb}/^{204}\text{Pb}$	σ	$^{207}\text{Pb}/^{204}\text{Pb}$	σ	$^{208}\text{Pb}/^{204}\text{Pb}$	σ
YP-1	Pyrite	18.221	0.003	15.625	0.003	38.416	0.009
YP-2	Pyrite	18.717	0.003	15.668	0.003	38.832	0.006
YP-3	Pyrite	18.886	0.003	15.684	0.002	39.695	0.008
YP-4	Pyrite	18.287	0.002	15.614	0.002	38.588	0.006
YP-5	Pyrite	18.176	0.002	15.594	0.002	38.324	0.005
YP-6	Pyrite	18.565	0.002	15.646	0.002	38.53	0.004
YP-7	Pyrite	18.249	0.003	15.687	0.002	38.568	0.006
YP-8	Pyrite	18.155	0.002	15.597	0.002	38.26	0.005
QC-1	Marble	23.035	0.006	16.146	0.004	37.668	0.011
QC-2	Marble	21.822	0.009	16.092	0.006	37.472	0.016
QC-3	Marble	22.314	0.013	16.128	0.01	37.623	0.021

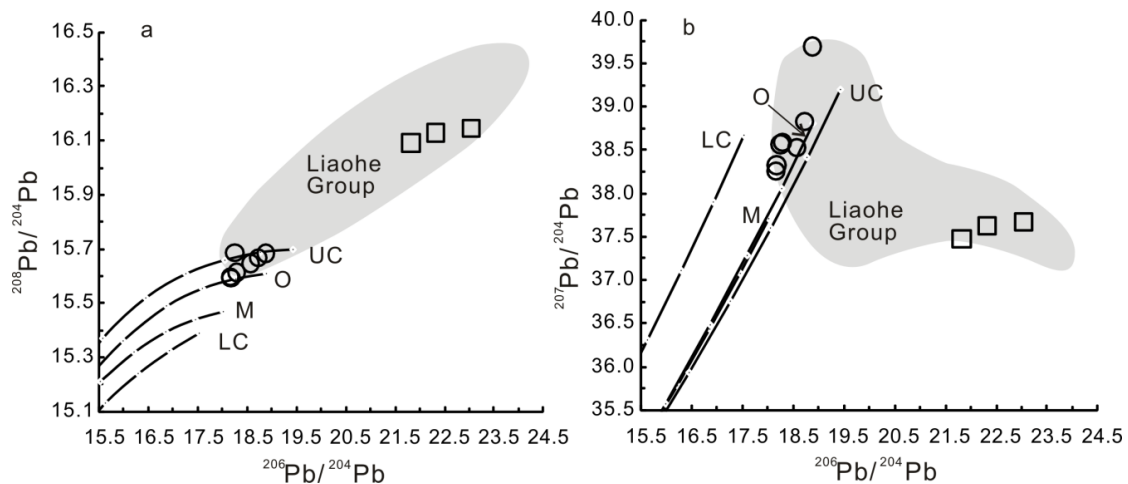


Figure 6. Lead isotope ratio from ore-bearing pyrite and marble from the Lijiapuzi deposit. Data of the Liaohe Group. (a) $^{208}\text{Pb}/^{204}\text{Pb}$ vs. $^{206}\text{Pb}/^{204}\text{Pb}$; and (b) $^{207}\text{Pb}/^{204}\text{Pb}$ vs. $^{206}\text{Pb}/^{204}\text{Pb}$. (Gaixian and Dashiqiao formations) are from [6].

4.4. S and Trace Element Compositions

A total of 37 spots on the two stages of pyrite from the Lijiapuzi gold deposit were selected for in situ LA-ICP-MS analysis of the sulfur and trace element compositions. The contents of the S and nine representative trace elements are presented in Supplementary Table S1.

Early-stage pyrite Py1, which often exhibits a euhedral cubic shape, has similar or slightly lower $\delta^{34}\text{S}$ contents than late-stage subhedral pyrite Py2 (Figure 7). The Py1 analysis spots yielded $\delta^{34}\text{S}$ values of +9.19‰ to +11.27‰, while the Py2 spots yielded $\delta^{34}\text{S}$ values of +9.49‰ to +11.49‰.

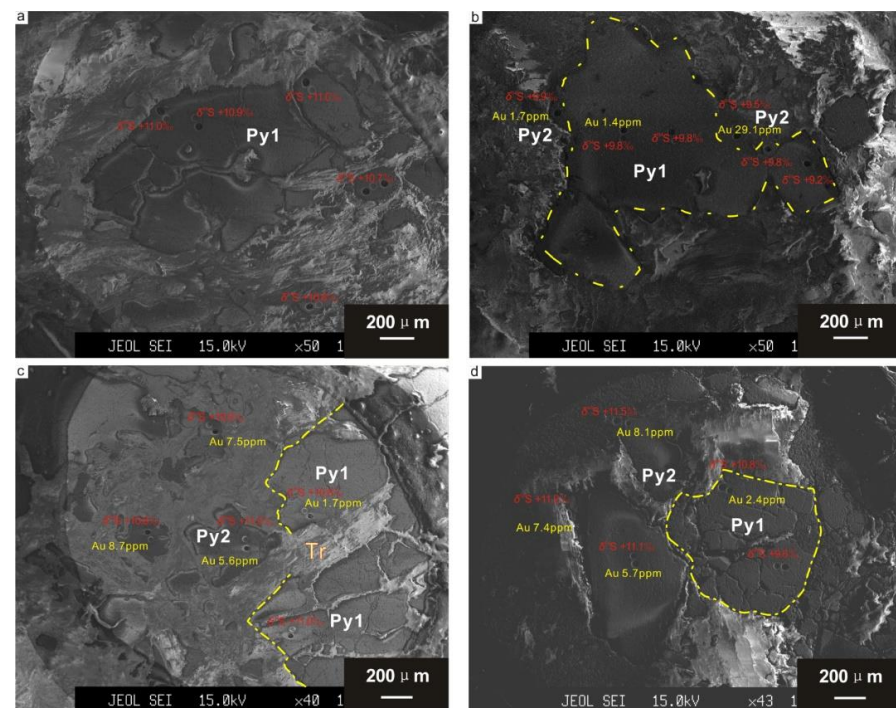


Figure 7. BSE images of ore-bearing pyrites in the Lijiapuzi deposit. In situ Au and $\delta^{34}\text{S}$ values are shown. (a) Early-stage pyrite with relatively low Au contents. (b–d) Py2 coexisted with tremolite distributing on the margin of early-stage pyrite. Py1—early-stage pyrite; Py2—late-stage pyrite; Tr—tremolite.

Gold and eight other gold-related trace element contents are shown in Figure 7. Compared to Py1, the Py2 shows higher Au, Sb, Cu, and Pb contents, slightly higher As and Ag contents, and similar Co, Ni, and Mo contents.

5. Discussion

5.1. Gold Metallogenic Epoch in the Lijiapuzi Deposit

The gold metallogenic epoch is usually determined through the dating of coexisting minerals, for instance, $^{40}\text{Ar}/^{39}\text{Ar}$ dating of biotite and muscovite, U–Pb zircon dating, and Re–Os and Rb–Sr dating of auriferous pyrite. Compared to biotite and muscovite, which have lower closure temperatures of ~ 350 °C, tremolite has an $^{40}\text{Ar}/^{39}\text{Ar}$ dating closure temperature of greater than 500 °C [42], so it can provide a much more reliable crystallization age, which is also indicative of the age of the gold metallogenic epoch.

The tremolite samples collected from the gold ore body in the Lijiapuzi gold deposit exhibit a paragenetic relationship with the auriferous pyrite (Py2) based on field and microscope observations (Figure 2). Thus, dating the tremolite could provide a robust constraint on the gold metallogenic epoch of the Lijiapuzi deposit. The $^{40}\text{Ar}/^{39}\text{Ar}$ dating of the tremolite yielded a plateau age of 1851.23 ± 12.8 Ma (Figure 4a). The similar isochronal line and inverse isochron ages of 1857.88 Ma and 1858.44 Ma, respectively, with an MSWD of 3.1, are even more persuasive (Figure 4b,c). These consistent dating results of ~ 1851 Ma could represent the crystallization age of tremolite, and thus, the gold metallogenic epoch of the Lijiapuzi deposit. This is the first Paleoproterozoic gold mineralization $^{40}\text{Ar}/^{39}\text{Ar}$ age reported for the Liaodong Peninsula.

5.2. Paleoproterozoic Gold Mineralization in the Lijiapuzi Deposit

Gold mineralization processes can be effectively constrained via the S–Pb isotope analysis of auriferous minerals because gold is often transported by sulfur-bearing complexes [44]. The sulfur isotope analyses of the auriferous pyrite yielded $\delta^{34}\text{S}$ values of +8.0‰ to +12.3‰, which differ from those of typical magmatic sulfur sources (Figure 5). Taking the geological setting of the deposit into consideration, the Paleoproterozoic meta-sedimentary country rocks of the Dashiqiao Formation are the most probable sulfur source of the Lijiapuzi gold deposit. The auriferous pyrite also yields lead isotopic ratios similar to those of the marbles of the Dashiqiao Formation and other Liaohe Group meta-sedimentary rocks based on previous studies (Figure 6) [6,8,38]. The country rock marbles of the Paleoproterozoic Liaohe Group provide ore-forming materials for the Lijiapuzi deposit.

In situ LA-ICP-MS sulfur and trace element analyses provide a new method for investigating the detailed mineralization processes of various mineral deposits [45–47]. Detailed observations under a microscope and EPMA studies revealed the presence of at least two stages of Au-bearing pyrite (Py1 and Py2). The Py1 grains exhibit euhedral-cubic or altered-cubic shapes, while the Py2 pyrite grains usually exhibit subhedral structures and are crystallized on the rim and/or near relics of the Py1 grains (Figure 7). Furthermore, the in situ S and trace element analyses of these types of pyrite revealed that they have relatively diverse compositions. Py1 (early-stage pyrite) has slightly lower $\delta^{34}\text{S}$ contents (Figure 5), while Py2 has higher gold, Sb, Cu, and Pb contents, slightly higher As and Ag contents, and similar Co, Ni, and Mo contents than Py1 (Figure 8). Thus, Py1 and Py2 could represent two gold mineralization stages. Py2, which coexists with tremolite, represents a main gold mineralization stage with high contents of Sb, Cu, and Pb.

5.3. Implications for Mineralization during the Jiao-Liao-Ji Orogeny

The JLJB in the NE NCC has a long and complex evolutionary history, consisting of a series of geological processes, including subduction, collision, accretion, and extension during the orogeny. The wide range of material exchange, water–rock reactions, and metamorphism were all favorable for the development of mineralizations [48,49]. In addition, the Paleoproterozoic sedimentary rocks of the Liaohe Group have relatively high gold contents of several ppm [13]. A gold mineralization model for the Paleoproterozoic

metamorphosed sedimentary rocks has been proposed by economic geologists [13–17], due to the similar distributions of the gold ore bodies and the Paleoproterozoic country rocks, as well as S and Pb isotope studies on the ore minerals and country rocks. The ~1851 Ma $^{40}\text{Ar}/^{39}\text{Ar}$ age and the related isotopic and geochemical data provide direct and robust constraints on the Paleoproterozoic gold mineralization in this region.

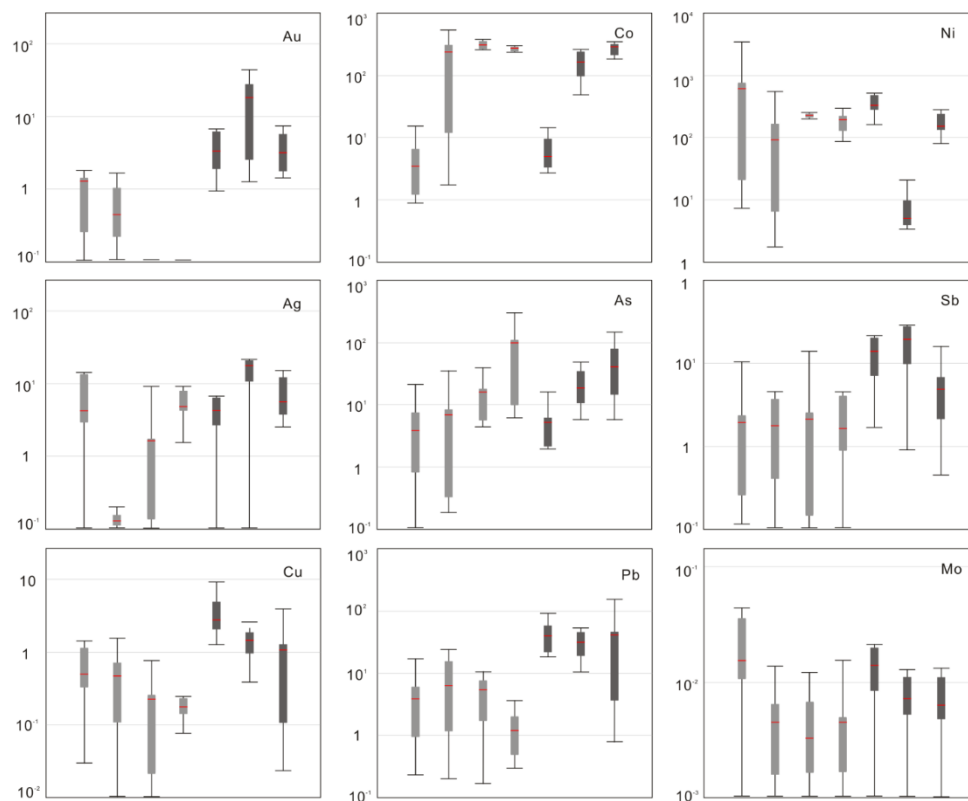


Figure 8. Box-and-whisker diagrams showing in situ Au, Co, Ni, Ag, As, Sb, Cu, Pb, and Mo from pyrite of the Lijiapuzi deposit. The red bar indicates the median value, the box encompasses the 25th to 75th percentiles of the data, and the whiskers indicate the minimum and maximum values. Light-grey bars show the Py1 spot data, while the dark-grey ones show the Py2 data.

Paleoproterozoic metallic mineralization in the Liaodong Peninsula was as remarkable as the undisputed nonmetallic boron and graphite deposition. Ma et al. [8] reported a sphalerite Rb–Sr age of 1798 ± 8 Ma from the Zhenzigou Pb–Zn deposit in the Qingchengzi orefield. Archean-banded iron formation (BIF) deposits in the Gongchangling area were also metamorphosed and experienced Fe enrichment at ~1860 Ma [50,51]. Taking the gold mineralization $^{40}\text{Ar}/^{39}\text{Ar}$ age of ~1851 Ma for the Lijiapuzi deposit into consideration, a widespread Au–Pb–Zn–Fe polymetallic mineralogenetic series was formed in the Qingchengzi–Liaoyang area in the central part of the JLJB. It is also noteworthy that the ~1860 to 1850 Ma metallogenic epoch was consistent with the regional retrograde metamorphism in the JLJB [27,33,52]. Extensive metamorphic fluids related to this large-scale metamorphism may have extracted ore materials from the meta-sedimentary country rocks, and then deposited them in the available spaces due to changes in the temperature and pressure and the involvement of meteoric water.

6. Conclusions

The tremolite plateau age of ~1851 Ma implies that Paleoproterozoic gold mineralization occurred in the Lijiapuzi gold deposit. Py2, coexisting with tremolite, represents the main gold mineralization stage accompanied with high contents of Sb, Cu, and Pb. A complex Paleoproterozoic mineralogenetic series of Au–Pb–Zn–Fe–B–graphite was identified in the Liaodong Peninsula. Further studies on Paleoproterozoic mineraliza-

tion and the evolutionary process of the JLJB orogeny could be a research highlight in this region.

Supplementary Materials: The following are available online at <https://www.mdpi.com/article/10.3390/min12080971/s1>, Table S1: In situ LA-ICP-MS S isotope and trace element compositions of pyrite from the Lijiapuzi gold deposit.

Author Contributions: Y.Z. conceived of and designed the ideas; P.Z. and L.K. tested the tremolite samples; Y.Z. and H.Y. analyzed the data; Y.Z., Z.B., Z.Y. and J.C. participated in the fieldwork; P.Z. and Y.Z. revised the manuscript. All authors have read and agreed to the published version of the manuscript.

Funding: This research was funded by National Key R&D Program of China grant number 2018YFC0603804; NSF of China, grant number 42072104; Geological Survey Project of China, grant number DD20221678, and the China Scholarship Council.

Acknowledgments: We thank the reviewers for their detailed work and constructive suggestions to improve the quality of this paper.

Conflicts of Interest: The authors declare no conflict of interest.

References

1. Zhao, G.C.; Sun, M.; Wilde, S.A.; Li, S.Z. Late Archean to Paleoproterozoic evolution of the North China Craton: Key issues revisited. *Precambr. Res.* **2005**, *136*, 177–202. [[CrossRef](#)]
2. Zhao, G.C.; Cawood, P.A.; Li, S.Z.; Wilde, S.A.; Sun, M.; Zhang, J.; He, Y.H.; Yin, C.Q. Amalgamation of the North China Craton: Key issues and discussion. *Precambr. Res.* **2012**, *222–223*, 55–76. [[CrossRef](#)]
3. Li, S.Z.; Zhao, G.C.; Sun, M.; Han, Z.Z.; Hao, D.F.; Luo, Y.; Xia, X.P. Deformation history of the Paleoproterozoic Liaohe Group in the Eastern Block of the North China Craton. *J. Asian Earth Sci.* **2005**, *24*, 659–674. [[CrossRef](#)]
4. Zhai, M.G.; Santosh, M. The early Precambrian odyssey of North China Craton: A synoptic overview. *Gondwana Res.* **2011**, *20*, 6–25. [[CrossRef](#)]
5. Xue, C.J.; Chen, Y.C.; Lu, Y.F.; Li, H.Q. Metallogenic epochs of Au and Ag deposits in Qingchengzi ore-clustered area, eastern Liaoning Province. *Miner. Depos.* **2003**, *22*, 177–184, (In Chinese with English abstract).
6. Yu, G.; Chen, J.F.; Xue, C.J.; Chen, Y.C.; Chen, F.K.; Du, X.Y. Geochronological framework and Pb, Sr isotope geochemistry of the Qingchengzi Pb–Zn–Ag–Au orefield, Northeastern China. *Ore Geol. Rev.* **2009**, *35*, 367–382. [[CrossRef](#)]
7. Zhao, Y.; Zhang, P.; Lv, J.C.; Zhang, S.; Kou, L.L.; Yang, Z.J. Characteristics of ore-forming fluids in the Gaojiapuzi Ag deposit of the Qingchengzi orefield, Liaoning Province and geological implications. *Geol. Explor.* **2015**, *51*, 441–450.
8. Ma, Y.B.; Bagas, L.; Xing, S.W.; Zhang, S.T.; Wang, R.J.; Li, N.; Zhang, Z.J.; Zou, Y.F.; Yang, X.Q.; Wang, Y.; et al. Genesis of the stratiform Zhenzigou Pb–Zn deposit in the North China Craton: Rb–Sr and C–O–S–Pb isotope constraints. *Ore Geol. Rev.* **2016**, *79*, 88–104. [[CrossRef](#)]
9. Yang, F.C.; Song, Y.H.; Zhang, P.; Chai, P.; Li, B. Forming fluid characteristics and tracing of ore-forming source materials of gold–silver deposit in the Qingchengzi ore concentration area. *Acta Geol. Sin.* **2016**, *90*, 2775–2785, (In Chinese with English abstract).
10. Zhao, Y.; Zhang, P.; Bi, Z.W. Key role of sedimentary formation played in the mineralization process of the Paleoproterozoic Yangmugan boron deposit in Liaodong Peninsula, NE China. *J. Earth Sci. Environ.* **2022**, *44*, 207–219, (In Chinese with English abstract).
11. Zeng, Q.D.; Chen, R.Y.; Yang, J.H.; Sun, G.T.; Yu, B.; Wang, Y.B.; Chen, P.W. The metallogenic characteristics and exploring ore potential of the gold deposits in eastern Liaoning Province. *Acta Petrol. Sin.* **2019**, *35*, 1939–1963.
12. Zhang, Z.C.; Wang, Y.W.; Li, D.D.; Lai, C. Lithospheric architecture and metallogenesis in Liaodong Peninsula, North China Craton: Insights from zircon Hf–Nd isotope mapping. *Minerals* **2019**, *9*, 179. [[CrossRef](#)]
13. Wang, Y.W.; Xie, H.J.; Li, D.D.; Shi, Y.; Liu, F.X.; Sun, G.Q.; Sun, Q.M.; Zhou, G.C. Prospecting prediction of ore concentration area exemplified by Qingchengzi Pb–Zn–Au–Ag ore concentration area, eastern Liaoning Province. *Miner. Depos.* **2017**, *36*, 1–24, (In Chinese with English abstract).
14. Liu, G.P.; Ai, Y.F. A discussion on some major problems of the Baiyun gold deposit, eastern Liaoning. *Miner. Depos.* **1999**, *18*, 219–225, (In Chinese with English abstract).
15. Song, J.C.; Hu, T.J.; Wang, E.D.; Jia, S.S. A comparison of metallogenic conditions between two sides of Yalu River and its inspiration to future ore-prospecting in Liaodong area. *Miner. Depos.* **2009**, *28*, 449–461, (In Chinese with English abstract).
16. Zhang, S.; Zhang, D.; Sha, D.X.; Kou, L.L.; Zhao, D.F. Metallogenic characteristics and genesis of the gold (silver) mineralization in Linjiasandaogou–Xiaotongjiapuzi area, eastern Liaoning Province. *J. Jilin Univ. (Earth Sci. Ed.)* **2012**, *42*, 725–732.

17. Song, Y.H.; Yang, F.C.; Yan, G.L.; Wei, M.H.; Shi, S.S. Characteristics of mineralization fluids and tracers of mineralization material sources of the Qingchengzi lead–zinc deposit in Liaoning Province. *Geol. Explor.* **2017**, *53*, 259–269, (In Chinese with English abstract).
18. Li, J.; Cai, W.Y.; Li, B.; Wang, K.Y.; Liu, H.L.; Konare, Y.; Qian, Y.; Lee, G.J.; Yoo, B.C. Paleoproterozoic SEDEX-type stratiform mineralization overprinted by Mesozoic vein-type mineralization in the Qingchengzi Pb–Zn deposit, Northeastern China. *J. Asian Earth Sci.* **2019**, *184*, 104009. [[CrossRef](#)]
19. Duan, X.X.; Zeng, Q.D.; Yang, J.; Liu, J.; Wang, Y.; Zhou, L.L. Geochronology, geochemistry and Hf isotope of Late Triassic magmatic rocks of Qingchengzi district in Liaodong Peninsula, Northeast China. *J. Asian Earth Sci.* **2014**, *91*, 107–124. [[CrossRef](#)]
20. Hao, L.B.; Zhao, X.; Zhao, Y.Y. Stable isotope characteristics and ore genesis of the Baiyun gold deposit, Liaoning Province. *J. Jilin Univ. (Earth Sci. Ed.)* **2017**, *47*, 442–451. [[CrossRef](#)]
21. Zhang, P.; Kou, L.L.; Zhao, Y.; Bi, Z.W.; Sha, D.M.; Li, Z.M.; Han, R.P. Fluid inclusions, H–O, S, Pb, and noble gas isotope studies of the Baiyun gold deposit in the Qingchengzi orefield, NE China. *J. Geochem. Explor.* **2019**, *200*, 37–53. [[CrossRef](#)]
22. Sun, G.T.; Zeng, Q.D.; Li, T.Y.; Li, A.; Wang, E.Y.; Xiang, C.S.; Wang, Y.; Chen, P.W.; Yu, B. Ore genesis of the Baiyun gold deposit in Liaoning province, NE China: Constraints from fluid inclusions and zircon U–Pb ages. *Arab. J. Geosci.* **2019**, *12*, 299. [[CrossRef](#)]
23. Yang, J.H.; Wu, F.Y.; Xie, L.W.; Liu, X.M. Petrogenesis and tectonic implications of Kuangdonggou syenites in the Liaodong peninsula, east North China Craton: Constraints from in-situ zircon U–Pb ages and Hf isotopes. *Acta Petrol. Sin.* **2007**, *23*, 263–276, (In Chinese with English abstract).
24. Tam, P.Y.; Zhao, G.C.; Liu, F.L.; Zhou, X.W.; Sun, M.; Li, S.Z. Timing of metamorphism in the Paleoproterozoic Jiao-Liao-Ji Belt: New SHRIMP U–Pb zircon dating of granulites, gneisses and marbles of the Jiaobei massif in the North China Craton. *Gondwana Res.* **2011**, *19*, 150–162. [[CrossRef](#)]
25. Chen, J.S.; Xing, D.H.; Liu, M.; Li, B.; Yang, H.; Tian, D.X.; Yang, F.; Wang, Y. Zircon U–Pb chronology and geological significance of felsic volcanic rocks in the Liaohe Group from the Liaoyang area, Liaoning Province. *Acta Petrol. Sin.* **2017**, *33*, 2792–2810, (In Chinese with English abstract).
26. Li, Z.; Chen, B.; Wei, C.J. Is the Paleoproterozoic Jiao-Liao-Ji Belt (North China Craton) a rift? *Int. J. Earth Sci.* **2017**, *106*, 355–375. [[CrossRef](#)]
27. Li, Z.; Li, J.; Chen, B. Early Precambrian tectonic-thermal events: Coupled U–Pb–Hf of detrital zircons from Jiao-Liao-Ji Belt, North China Craton. *Arab. J. Geosci.* **2018**, *11*, 424–440. [[CrossRef](#)]
28. Liu, J.; Zhang, J.; Liu, Z.H.; Yin, C.Q.; Zhao, C.; Li, Z.; Yang, Z.J.; Dou, S.Y. Geochemical and geochronological study on the Paleoproterozoic rock assemblage of the Xiuyan region: New constraints on an integrated rift-and-collision tectonic process involving the evolution of the Jiao-Liao-Ji Belt, North China Craton. *Precamb. Res.* **2018**, *310*, 179–197. [[CrossRef](#)]
29. Zhao, Y.; Kou, L.L.; Zhang, P.; Bi, Z.W.; Li, D.T.; Chen, C. Characteristics of Geochemistry and Hf isotope from meta-gabbro in the Longchang area, eastern of North China Craton: Implications on the evolution of the Jiaoliaoji Paleoproterozoic orogeny belt. *Earth Sci.* **2019**, *44*, 3333–3345, (In Chinese with English abstract).
30. Zhu, R.X.; Fan, H.R.; Li, J.W.; Meng, Q.R.; Li, S.R.; Zeng, Q.D. Decratonic gold deposits. *Sci. China Earth Sci.* **2015**, *58*, 1523–1537. [[CrossRef](#)]
31. Song, Y.H.; Yang, F.C.; Yan, G.L.; Wei, M.H.; Shi, S.S. SHRIMP U–Pb ages and Hf isotopic compositions of Paleoproterozoic granites from the Eastern part of Liaoning Province and their tectonic significance. *Acta Geol. Sin.* **2016**, *90*, 2620–2636, (In Chinese with English abstract).
32. Wang, X.P.; Peng, P.; Wang, C.; Yang, S.Y. Nature of three episodes of Paleoproterozoic magmatism (2180 Ma, 2115 Ma and 1890 Ma) in the Liaoji belt, North China with implications for tectonic evolution. *Precamb. Res.* **2017**, *298*, 252–267. [[CrossRef](#)]
33. Zhao, Y.; Zhang, P.; Li, Y.; Li, D.T.; Chen, J.; Bi, Z.W. Geochemistry of two types of Paleoproterozoic granites, and zircon U–Pb dating, and Lu–Hf isotopic characteristics in the Kuandian area within the Jiao-Liao-Ji Belt: Implications for regional tectonic setting. *Geol. J.* **2020**, *55*, 7564–7580. [[CrossRef](#)]
34. Zhao, Y.; Lin, S.F.; Zhang, P. Geochronology and geochemical characteristics of Paleoproterozoic syn-orogenic granitoids and constraints on the geological evolution of the Jiao-Liao-Ji orogenic belt, North China Craton. *Precamb. Res.* **2021**, *365*, 106386. [[CrossRef](#)]
35. Wang, X.P.; Peng, P.; Wang, C.; Yang, S.Y. Petrogenesis of the 2115 Ma Haicheng mafic sills from the Eastern North China Craton: Implications for an intra-continental rifting. *Gondwana Res.* **2016**, *39*, 347–364. [[CrossRef](#)]
36. Xu, W.; Liu, F.L.; Tian, Z.H.; Liu, L.S.; Ji, L.; Dong, Y.S. Source and petrogenesis of Paleoproterozoic meta-mafic rocks intruding into the North Liaohe Group: Implications for back-arc extension prior to the formation of the Jiao-Liao-Ji Belt, North China Craton. *Precamb. Res.* **2018**, *207*, 66–81. [[CrossRef](#)]
37. Duan, X.X.; Zeng, Q.D.; Wang, Y.B.; Zhou, L.L. Genesis of the Pb–Zn deposits of the Qingchengzi ore field, eastern Liaoning, China: Constraints from carbonate LA-ICPMS trace element analysis and C–O–S–Pb isotopes. *Ore Geol. Rev.* **2017**, *89*, 752–771. [[CrossRef](#)]
38. Zhao, Y.; Yang, H.Z.; Yang, F.C.; Zhang, P.; Gu, Y.C.; Xu, J. Genesis of the typical gold deposits in Qingchengzi orefield, Liaodong Peninsula: Evidences from S–D–O isotopes. *Geol. Res.* **2020**, *29*, 21–28, (In Chinese with English abstract).
39. Liu, J.; Liu, F.X.; Li, S.H.; Lai, C.K. Formation of the Baiyun gold deposit, Liaodong gold province, NE China: Constraints from zircon U–Pb age, fluid inclusion, and C–H–O–Pb–He isotopes. *Ore Geol. Rev.* **2019**, *104*, 686–706. [[CrossRef](#)]

40. Zhang, Y.; Chen, W.; Chen, K.L.; Liu, X.Y. Study on the Ar-Ar age spectrum of diagenetic I/S and the mechanism of ^{39}Ar recoil loss—Examples from the clay minerals of P-T boundary in Changxing, Zhejiang Province. *Geol. Rev.* **2006**, *52*, 556–561.
41. Liu, Y.S.; Hu, Z.C.; Gao, S.; Günther, D.; Xu, J.; Gao, C.G.; Chen, H.H. In situ analysis of major and trace elements of anhydrous minerals by LA-ICP-MS without applying an internal standard. *Chem. Geol.* **2008**, *257*, 34–43. [[CrossRef](#)]
42. Thern, E.R.; Blereau, E.; Jourdan, F.; Nelson, D.R. Tourmaline $^{40}\text{Ar}/^{39}\text{Ar}$ geochronology and thermochronology: Example from the youngest Hadean-zircon-bearing siliciclastic metasedimentary rocks from the Yilgarn Craton. *Geochim. Cosmochim. Acta* **2020**, *27*, 285–299. [[CrossRef](#)]
43. Hoefs, J. *Stable Isotope Geochemistry*, 3rd ed.; Springer: Berlin, Germany, 1986; p. 241.
44. Zhao, H.X.; Frimmel, H.E.; Jiang, S.Y.; Dai, B.Z. LA-ICP-MS trace element analysis of pyrite from the Xiaoqinling gold district, China: Implications for ore genesis. *Ore Geol. Rev.* **2011**, *43*, 142–153. [[CrossRef](#)]
45. Zhang, J.; Deng, J.; Chen, H.Y.; Yang, L.Q.; Cooke, D.; Danyushevsky, L.; Gong, Q.J. LA-ICP-MS trace element analysis of pyrite from the Chang’an gold deposit, Sanjiang region, China: Implication for ore-forming process. *Gondwana Res.* **2014**, *26*, 557–575. [[CrossRef](#)]
46. Wen, G.; Li, J.W.; Hofstra, A.H.; Koenig, A.E.; Lowers, H.A.; Adams, D. Hydrothermal reequilibration of igneous magnetite in altered granitic plutons and its implications for magnetite classification schemes: Insights from the Handan-Xingtai iron district, North China Craton. *Geochim. Cosmochim. Acta* **2017**, *213*, 255–270. [[CrossRef](#)]
47. Yang, L.; Wang, Q.F.; Large, R.R.; Mukherjee, I.; Deng, J.; Li, H.J.; Yu, H.Z.; Wang, X. Fluid source and metal precipitation mechanism of sediment-hosted Chang’an orogenic gold deposit, SW China: Constrains from sulfide texture, trace element, S, Pb and He-Ar isotopes and calcite C-O isotopes. *Am. Mineral.* **2021**, *106*, 410–429. [[CrossRef](#)]
48. Yang, L.; Wang, Q.F.; Groves, D.I.; Lu, S.; Li, H.J.; Wang, P.; Deng, J. Multiple orogenic gold mineralization events in a collisional orogen: Insights from an extruded terrane along the southeastern margin of the Tibetan Plateau. *J. Struct. Geol.* **2021**, *147*, 104333. [[CrossRef](#)]
49. Yang, L.; Wang, Q.F.; Large, R.R.; Fougereuse, D.; Mukherjee, I.; Zhang, Q.Z.; Deng, J. Texture and geochemistry of pyrite from the Jinya, Nakuang and Gaolong gold deposits in the Youjiang Basin: Implications for basin-scale gold mineralization. *Min. Deposita* **2022**, 1–24. [[CrossRef](#)]
50. Li, H.M.; Liu, M.J.; Li, L.X.; Yang, X.Q.; Yao, L.D.; Chen, J.; Yao, T. SHRIMP U-Pb geochronology of zircons from the garnet-rich altered rocks in the mining area of the Gongchangling iron deposit: Constraints on the ages of the high-grade iron deposit. *Acta Petrol. Sin.* **2014**, *30*, 1205–1217.
51. Li, L.X.; Zi, J.W.; Li, H.M.; Rasmussen, B.; Wilde, S.A.; Sheppard, S.; Ma, Y.B.; Meng, J.; Song, Z. High-Grade magnetite mineralization at 1.86 Ga in Neoproterozoic banded iron formations, Gongchangling, China: In situ U-Pb geochronology of metamorphic-hydrothermal zircon and monazite. *Econ. Geol.* **2019**, *114*, 1159–1175. [[CrossRef](#)]
52. Liu, P.H.; Liu, F.L.; Yang, H.; Wang, F.; Liu, J.H. Protolith ages and timing of peak and retrograde metamorphism of the high pressure granulites in the Shandong Peninsula, eastern North China Craton. *Geosci. Front.* **2012**, *3*, 923–943. [[CrossRef](#)]